Chinese Chemical Letters 37 (2026) 111736

Contents lists available at ScienceDirect

Chinese Chemical Letters

journal homepage: www.elsevier.com/locate/cclet

Arene-perfluoroarene force driven chiral transfer, chiral amplification and chiral inversion

Bo Luo[a], Mingfang Ma[b,*], Aiyou Hao[c], Pengyao Xing[c,*]

[a] Henan Key Laboratory of Tea Plant Biology, College of Tea and Food Science, Xinyang Normal University, Xinyang 464000, China
[b] College of Basic Medicine & Laboratory of New Antitumor Drug Molecular Design and Synthesis of Jining Medical University & Jining Key Laboratory of Pharmacology, Jining Medical University, Jining 272067, China
[c] School of Chemistry and Chemical Engineering, Shandong University, Ji'nan 250100, China

ARTICLE INFO

Article history:
Received 19 July 2024
Revised 5 August 2025
Accepted 17 August 2025
Available online 17 August 2025

Keywords:
Arene-perfluoroarene interaction
Circularly polarized luminescence
Chirality transfer
Chiral amplification
Chiral inversion

ABSTRACT

Co-assembling chiral molecules with achiral compounds *via* non-covalent interactions like arene-perfluoroarene (AP) interactions offers an effective approach for fabricating chiral functional materials. Herein, chiral molecules **L/D-PF1** and **L/D-PF2** with pyrene groups were synthesized and its chiroptical properties upon co-assembly with achiral compound octafluoronaphthalene (OFN) through AP interaction were systemically studied. The co-assembly of **L/D-PF1**/OFN and **L/D-PF2**/OFN exhibited distinct chiroptical properties such as circular dichroism (CD) and circularly polarized luminescence (CPL) signals. Chirality transfer from the chirality center of **L/D-PF1** and **L/D-PF2** to the achiral OFN and chiral amplification were successfully achieved. Besides, no significant CPL signal was observed in the self-assembly of **L/D-PF1** or **L/D-PF2** while co-assembly with OFN exhibited obvious CPL amplification induced by AP interaction. Notably, a reversal CD signal and CPL signal could be observed in **L/D-PF2**/OFN when the molar ratio changed from 1:1 to 1:2 while not found in **L/D-PF1**/OFN, indicating that that minor structural changes of molecules could cause large changes in assembly. In addition, a series of computational calculations were conducted to verify the AP interaction between **L-PF1**/**L-PF2** and OFN. This work demonstrated that arene-perfluoroarene interaction could drive chiral transfer, chiral amplification and chiral inversion and provided a new method for the preparation of chiroptical materials.

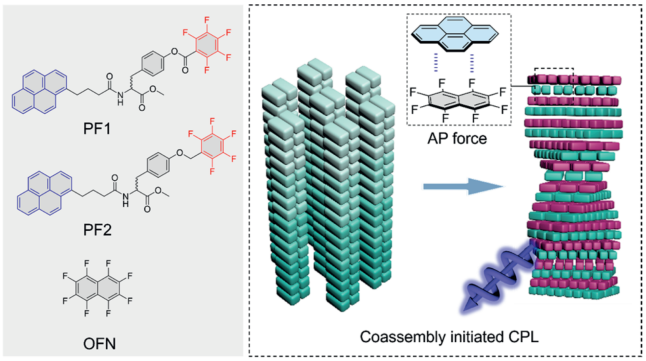
© 2025 Published by Elsevier B.V. on behalf of Chinese Chemical Society and Institute of Materia Medica, Chinese Academy of Medical Sciences.

Chirality describes the geometric characteristic of a rigid object that cannot be overlapped with its mirror image. Typically, chiral objects have two distinct forms, known as enantiomers in the field of chemistry [1]. Chirality holds great importance across various domains, particularly in biological systems. Here, enantiopure biomolecules like L-amino acids and D-sugars are fundamental building blocks for creating intricate biomacromolecules such as helical proteins and DNA. Thus, chirality emerges as a fundamental aspect of life, spanning from the molecular to the supramolecular scale [2,3]. Chiral supramolecular complexes, arising from hierarchical assembly of either chiral molecular components or achiral building blocks, represent significant trends in supramolecular chemistry and materials science, attributed to their fascinating properties [4–8]. Specifically, Chiral π-conjugated molecules or self-assembled structures demonstrate not only the inherent properties of conjugated absorption, fluorescence, and electron delocalization, but also additional features like CPL absorption and specific recognition [9–12]. The distinctive attributes of chiral π-conjugated structures pave the path for diverse innovative applications, including the generation or detection of CPL [13–17], asymmetric catalysis [18], chiroptical switches [19,20], chiral recognition [21–25], and chiral optoelectronic materials [26]. Precise and deliberate manipulation of supramolecular chirality across various scales holds promise in materials design, yet it remains a notably daunting task.

The combination of chiral molecules and achiral compounds in supramolecular co-assembly provides an effective method for creating chiral functional materials *via* non-covalent interactions like π–π stacking, hydrogen bonds, host–guest interactions, and electrostatic interactions among diverse building blocks [27–32]. Among them, the arene-perfluoroarene (AP) interaction represents a specific form of electrostatic interaction involving a perfluoroarene as the π acceptor and a non-fluorinated aromatic ring as the π donor [33–36]. The AP interaction has been regarded as a significant non-covalent force in the realms of supramolecular chemistry, crystal engineering, and materials science, which offers

* Corresponding authors.
E-mail addresses: mamingfang2012@163.com (M. Ma), xingpengyao@sdu.edu.cn (P. Xing).

https://doi.org/10.1016/j.cclet.2025.111736
1001-8417/© 2025 Published by Elsevier B.V. on behalf of Chinese Chemical Society and Institute of Materia Medica, Chinese Academy of Medical Sciences.



Scheme 1. Molecular structure of building units and structural evolution of the two building units driven by AP interaction.

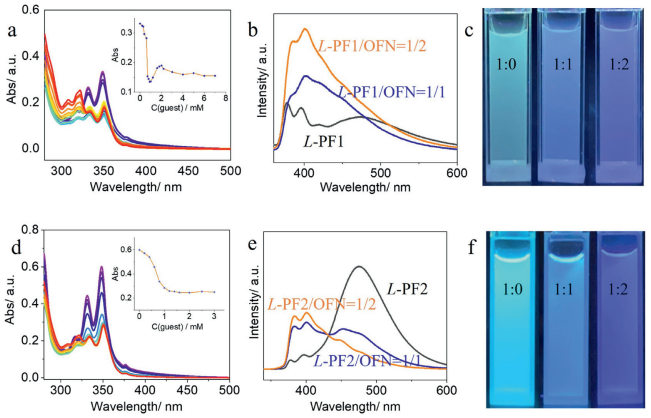


Fig. 1. (a) UV spectra comparison of self-assembly and co-assembly of L-**PF1** with OFN at different configurations. (b) Fluorescence spectra of L-**PF1**/OFN = 1/0∼1/2. (c) Luminescence colors of L-**PF1**/OFN = 1/0∼1/2 under a 365 nm light. (d) UV spectra comparison of self-assembly and co-assembly of L-**PF2** with OFN at different configurations. (e) Fluorescence spectra of L-**PF2**/OFN = 1/0∼1/2. (f) Luminescence colors of L-**PF2**/OFN = 1/0∼1/2 under a 365 nm light. Concentrations of L-**PF1**/OFN and L-**PF2**/OFN were 0.01 and 0.05 mmol/L, respectively.

advantages for the regulation of optical and electronic properties of organic compounds [37–39]. Recently, octafluoronaphthalene (OFN) has been used as a molecular barrier to intercalate into matrices of organic aromatic fluorophores, with the goal of enhancing the emission efficiency of polycyclic aromatic hydrocarbons (PAHs) such as tetracene, perylene, pyrene, coronene, anthracene and phenazine [40–44]. For instance, our group designed and synthesized a series of pyrene-conjugated amino acids, pyrene-carboxylic acid-benzimidazole derivatives and perylene-conjugated peptoids. The results showed that these pyrene/perylene derivatives could form co-assemblies with OFN *via* AP interaction and induced the emergence of macroscopic chirality and CPL, which enriched the handedness of chiroptical active materials and functional chiral composites design [45–47]. Recently, two chiral molecules bearing pyrene and OFN though alanine were designed and synthesized by our group and their chiroptical properties upon self-assembly were studied. The results indicated that selective chiral dimerization and folding could achieve by intramolecular AP interactions, suggesting that chiral architectures at different hierarchical levels could be manipulated *via* AP interactions [48]. In this work, we designed and synthesized four molecules L/D-**PF1** and L/D-**PF2** with pyrene groups as π donor and pentafluorophenyl group as π acceptor. We envisioned that these compounds generated a chiral tweezer to include guests *via* intramolecular AP interactions. However, experimental and computational results indicated that these compounds did not form the desired chiral tweezers but self-assembled into some other superstructures like sheets or fibers *via* π–π stacking between pyrenes. This might due to the intermolecular AP interactions between pyrene groups and pentafluorophenyl group were weaker than the π–π stacking between pyrenes. To continue our work, OFN was introduced to co-assembly with the synthesized molecules. The results showed that co-assembly L/D-**PF1** with OFN could form spiral fibers and amplified CPL. On the other hand, co-assembly L/D-**PF2** with OFN could form chiral tweezers to include guest as OFN *via* intermolecular AP interactions. This difference might due to the fact that the rigid ester group fixed L/D-**PF1** to a linear conformation while flexible ether allowed the L/D-**PF2** molecules to fold into a tweezer structure. These results suggested that minor structural changes of molecules could cause large changes in assembly (Scheme 1).

Ultraviolet (UV) titration was conducted to explore molar ratio of the assemblies by fixing the concentration of L-**PF1** (0.01 mmol/L) and L-**PF2** (0.05 mmol/L) and gradually increasing the proportion of OFN (Figs. 1a and d). For L-**PF1**, increasing molar ratio of OFN witnessed the gradual decrease of UV absorption at peak of 348 nm until the molar ratio reached to 1:1. After that, the UV absorption increased until the molar ratio arrived at 1:2 and then the UV absorption remained unchanged (Fig. 1a). For L-**PF2**, with the addition of OFN, the UV absorption decreased at peak of 348 nm until the molar ratio reached to 1:1 and then keep unchanged (Fig. 1d). These results indicated the optimal proportion of L-**PF1** and OFN was about 1:2 while 1:1 for L-**PF2**/OFN. To inspect the optical properties, fluorescence of self-assembly and co-assembly were measured (Figs. 1b and e). L-**PF1** and L-**PF2** exhibited cyan fluorescence under 365 nm illumination, peaking at 475 nm. Upon co-assembly with OFN, the fluorescence of L-**PF1/OFN** and L-**PF2/OFN** shifted to blue, with an emission peak around 400 nm (Figs. 1c and f), indicating AP interaction formation accompanied by a blue-shift in emission wavelength. We also tested the fluorescence quantum yield (QY) of L-**PF1** and L-**PF2**, which was 1.05 % and 8.83 %, respectively (Fig. S9 in Supporting information). This difference might be caused by the slight structural differences between them.

To explore the development of supramolecular chirality resulting from assembly, CD was conducted following an incubation period of at least 8 h under ambient conditions (Figs. 2a-d). The CD spectra of L/D-**PF1** showed apparent Cotton effects at 288 nm and 360 nm. After co-assembling with OFN, the Cotton effects of L/D-**PF1** decreased, while new Cotton effects emerged at 228 nm and 353 nm. With the concentration of OFN increased, the CD intensity of L/D-**PF1**/OFN exhibited an initial increase followed by a decrease, reaching a maximum at a 1:2 molar ratio, consistent with the result of UV titration. This phenomenon demonstrated that the successful chirality transfer from the chiral center of L/D-**PF1** to the achiral OFN was achieved. A similar trend was also noted for L/D-**PF2**/OFN, with the original Cotton effects of L/D-**PF2** being almost nothingness, and the highest CD intensity appeared at a 1:1 molar ratio, which was also in agreement with the result of UV titration. Notably, a reversal phenomenon could be observed in L/D-**PF2**/OFN when the molar ratio changed from 1:1 to 1:2. These results indicated co-assembly with OFN led to chirality transfer and chirality amplification. To explore alterations in chiroptical properties due to assembly behavior, CPL experiments were conducted (Figs. 2e-h). Self-assembly of L/D-**PF1** did not yield significant CPL signals, whereas co-assembly with OFN showed obvious CPL properties with an evident hypsochromic shift attributed to AP interactions. The dissymmetry factor g_{lum} was around 3.7×10^{-3} (L/D-**PF1**/OFN = 1/1) and 5.5×10^{-3} (L/D-**PF1**/OFN = 1/2), respectively. Similarly, self-assembly of L/D-**PF2** did not exhibit significant CPL signals initially. Nevertheless, upon induction by AP interactions, they all demonstrated promi-

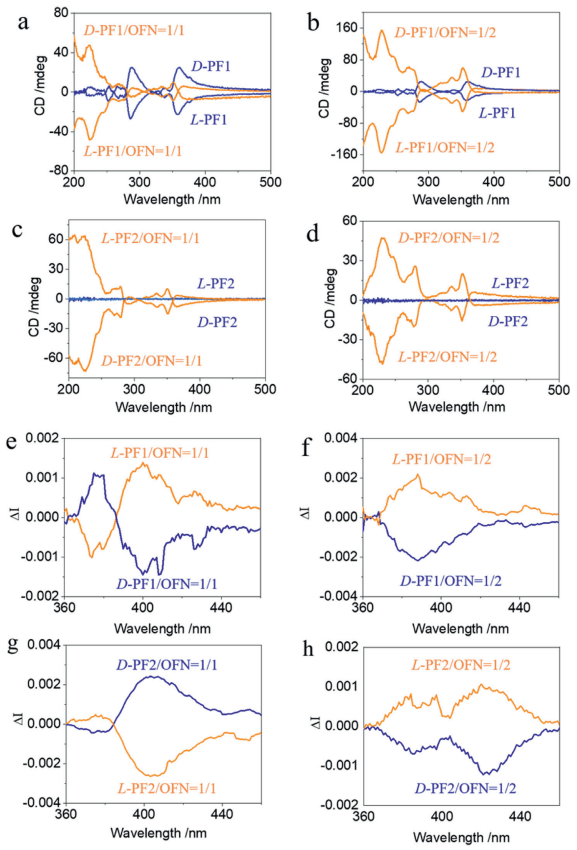


Fig. 2. (a–d) CD spectra comparison of self-assembly and co-assembly of different configurations. CPL spectra comparison of assemblies: (e) **L/D-PF1**/OFN =1/1; (f) **L/D-PF1**/OFN = 1/2; (g) **L/D-PF2**/OFN = 1/1; (h) **L/D-PF2**/OFN = 1/2; λex = 340 nm and 320 nm, respectively. Concentrations of **L/D-PF1** and **L/D-PF2** were 0.5 mmol/L.

nent CPL signals, with g_{lum} reaching 6.3×10^{-3} (**L/D-PF2**/OFN = 1/1) and 1.7×10^{-3} (**L/D-PF2**/OFN = 1/2). Notably, a reversal CPL signal was observed in **L/D-PF2**/OFN when the molar ratio changed from 1:1 to 1:2, which was in accordance with Cotton effects. Upon addition of OFN molecules, strong AP interactions between **L/D-PF2** and OFN induce changes in the molecular packing of **L/D-PF2**, leading to a dramatic transformation in the aggregate morphology. As revealed by TEM images, at a 1:1 ratio, the macroscopic structure evolves from bundled fibers to dispersed. When the ratio is further increased to 1:2, spherical structures become predominant. This demonstrates the transformation of **L-PF2** from fibrous to spherical structures. The assembly of **L-PF1** and OPF at a 1:1 ratio represents an intermediate state. CD and CPL are statistical measurements. Only a small fraction of spherical structures is present, results in chiroptical signals characteristic of the intermediate state. When the ratio is increased to 1:2, the spherical structures become predominant, and the observed chiroptical properties reflect this morphology. This explains the reversal of the CPL and CD signals. These findings demonstrated that the co-assembly of **L/D-PF1** and **L/D-PF2** with OFN resulted in novel morphology and chiroptical properties, offering a novel approach to preparing chiroptical materials.

To reveal the morphology of the assemblies, the scanning electron microscopy (SEM) and transmission electron microscopy (TEM) were recorded (Fig. 3). Self-assembly of **L-PF1** showed lamella structures while **L-PF2** individually displayed fiber structures, indicating that minor structural difference of molecules led to great change of aggregate morphologies. After co-assembly with OFN, **L-PF1**/OFN exhibited spiral fibers when the molar ratio was

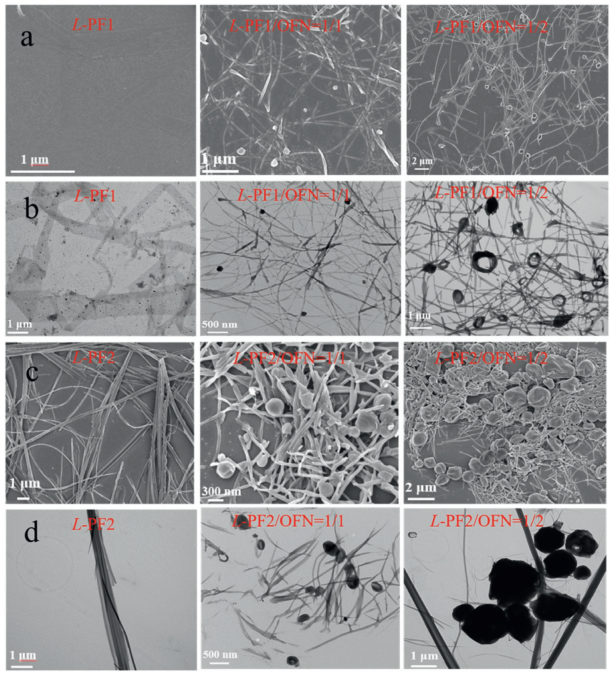


Fig. 3. SEM images of self-assembly and co-assembly of **L-PF1** (a) and **L-PF2** (c). TEM images of self-assembly and co-assembly of **L-PF1** (b) and **L-PF2** (d). Concentrations of **L-PF1**/**L-PF2** and OFN were 0.5 mmol/L.

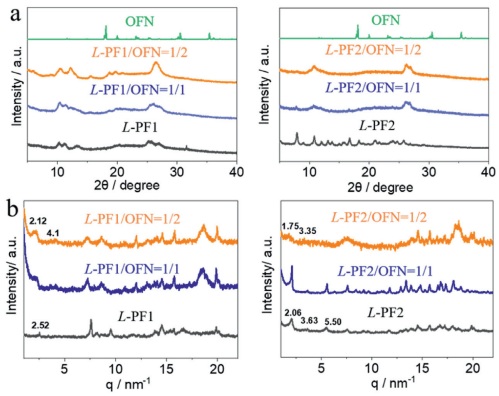


Fig. 4. (a) XRD patterns comparison of self-assembly and co-assembly. (b) SAXS spectral comparison self-assembly and co-assembly.

1:1 and it further evolved into a spiral coil at one top of the spiral fibers when the molar ratio arrived at 1:2. As for **L-PF2**, OFN participation produced spherical microparticles when the molar ratio was 1:1 and the number of spheroidal structures increased when the molar ratio reached 1:2. These results further demonstrated that minor structural changes of molecules could cause large changes in assembly.

In order to describe the molecular assembly structures, X-ray powder diffraction (XRD) and small angle X-ray scattering (SAXS) were exploited to reveal the variations in molecular arrangement caused by the noncovalent bonds in different assemblies. XRD patterns comparison on the **L-PF1** with OFN indicates the retainment of most diffraction patterns with however shifted bands. It suggests the partial social co-aggregation between the two components (Fig. 4a). And no individual diffraction peaks of OFN were found, which were assumably embedded in the molecular arrangement to afford new type of self-assembly arrays. Individual **L-PF2** possesses several sharp peaks as the formation of well-ordered molecular packing, which however were replaced by the

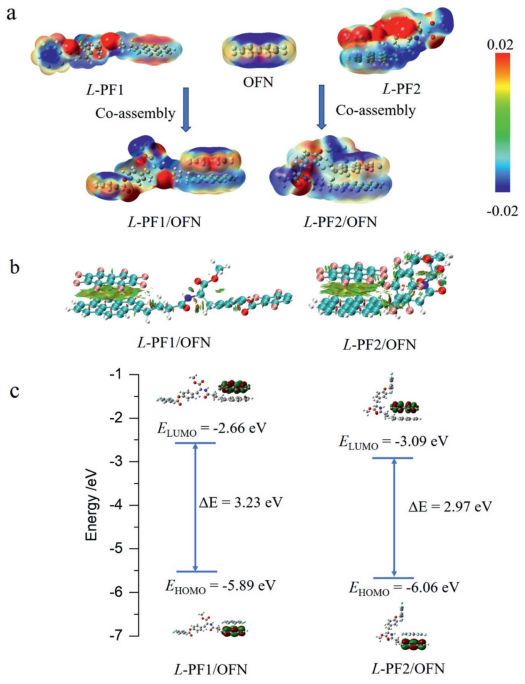


Fig. 5. (a) Electrostatic potential maps of **L-PF1**/OFN and **L-PF2**/OFN. (b) Non-covalent interaction calculations of **L-PF1**/OFN and **L-PF2**/OFN. (c) Density functional theory calculations **L-PF1**/OFN and **L-PF2**/OFN.

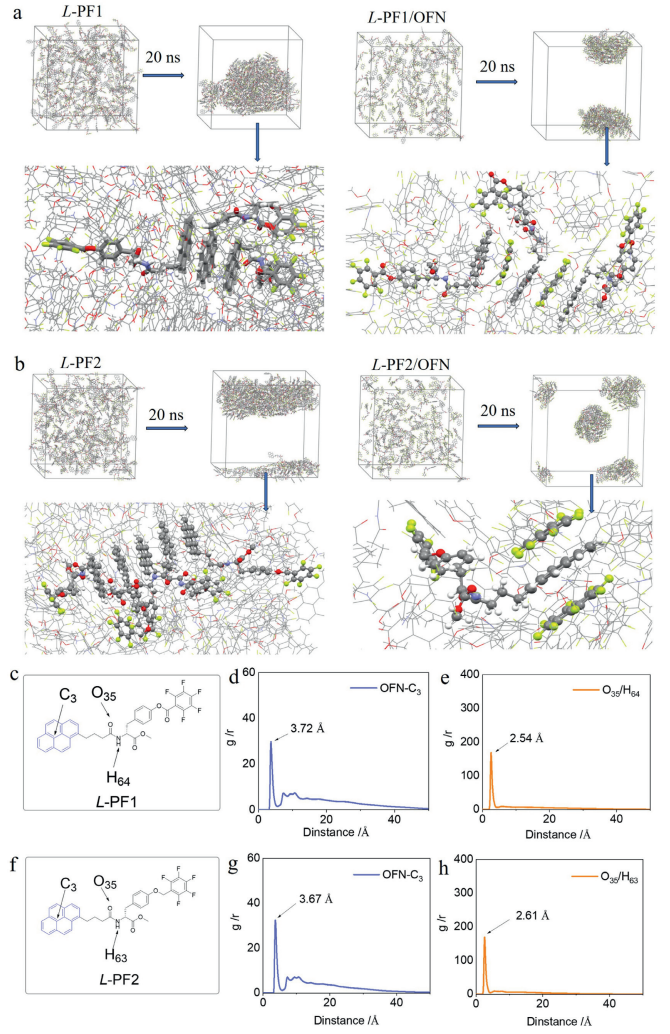


Fig. 6. (a) MD results (20 ns) of **L-PF1** and **L-PF1**/OFN. (b) MD results (20 ns) of **L-PF2** and **L-PF2**/OFN. (c) Atomic number assignment of **L-PF1**. RDF profiles of distances about (d) AP interaction between **L-PF1** and OFN, (e) H-bonds between O_{35} and H_{64} and (f) atomic number assignment of **L-PF2**. RDF profiles of distances about (g) AP interaction between **L-PF2** and OFN and (h) H-bonds between O_{35} and H_{63}.

hump peaks after incorporating OFN, implying the extended one-dimensional aggregation with higher aspect ratios. SAXS patterns give information regarding the mesophase molecular stackings (Fig. 4b). The primary peak at 2.52 $Å^{-1}$ transforms into new bands at 2.1 and 4.1 $Å^{-1}$ respectively, which suggests the formation of lamellar phase with OFN. In case of **L-PF2**, the primary three bands at 2.06, 3.63 and 5.50 $Å^{-1}$ correspond to the ratio of 1: $\sqrt{3}$: $\sqrt{7}$, corresponding to a well-defined hexagonal packing mode. After incorporating two molar equiv. OFN, the primary bands were replaced by a set of new bands at 1.75 and 3.35 $Å^{-1}$ respectively, which is assigned as the lamellar structure. OFN with strong AP interaction induces the phase transformation.

Computational calculations were performed to confirm the AP interaction between **L-PF1**/**L-PF2** and OFN. Electrostatic potential maps (ESP) of **L-PF1**/**L-PF2**, OFN, and their co-assembly were calculated using the B3LYP-D3(BJ)/6–311G-(d,p) level of theory (Fig. 5a). The results showed the central region of OFN formed an electrophilic π-hole while the central region of pyrene formed an electron-rich region due to pronounced electronegativity disparities between hydrogen and fluorine atoms, which allowed them to interact easily *via* AP interaction. It is worth noting that the pentafluorophenyl group of **L-PF2** could also interact with OFN *via* π-hole and fluorine atoms, which could fix the tweezer structure. A major gravitational interaction between **L-PF1**/**L-PF2** and OFN was further conformed by the non-covalent interaction (NCI) calculations (Fig. 5b). The density functional theory (DFT) calculations showed that the HOMO of **L-PF1**/**L-PF2** mainly located on the pyrene ring, while the LUMO mainly distributes on the OFN, suggesting that the electrons was transferred from the pyrene rings of **L-PF1**/**L-PF2** to OFN. The energy gaps of **L-PF1**/OFN and **L-PF2**/OFN were around 3.23 and 2.97 eV, which indicated there might be some difference between **L-PF1** and **L-PF2** due to molecular structures (Fig. 5c).

Molecular dynamic simulation (MD) was further employed to visualize the non-covalent bonds of self-assembly and co-assembly. 200 molecules of **L-PF1** or **L-PF2** were placed into a simulation box measuring $10 \times 10 \times 10$ nm^3. The system was allowed to equilibrate in water for a duration of 20 nanoseconds. And the co-assembly of **L-PF1** or **L-PF2** with OFN followed a similar procedure, employing a 1:1 molar ratio and utilizing a simulation box of dimensions $10 \times 10 \times 10$ nm^3 (Figs. 6a and b). The MD results demonstrated that self-assembled into aggregates *via* π-π stacking between pyrene planes and the introduce of OFN significantly changed the stacking between pyrene by AP interactions. Radial distribution function (RDF) maps were collected and the results were showed in Figs. 6d–h. Figs. 6d and g demonstrated the distances between pyrene of **L-PF1**/**L-PF2** and OFN. The prominent peaks at 3.72 and 3.67 Å suggested a high likelihood of AP interaction occurring. The possibility of hydrogen bonds between O_{35} and H_{64} of **L-PF1** (Fig. 6e) and hydrogen bonds between O_{35} and H_{63} of **L-PF2** (Fig. 6h) were also calculated. The distance at 2.54 and 2.61 Å evidenced the presence of weak hydrogen bonds during the self-assembly and the co-assembly. These findings suggested that the introduction of OFN led to a notable reduction in π-stacking interactions among perylene moieties, implying that OFN intercalated within the arrangement of perylene moieties.

In summary, chiral molecules **L/D-PF1** and **L/D-PF2** with pyrene groups were synthesized and its chiroptical properties upon co-

assembly with achiral compound OFN through AP interaction between pyrene moiety and OFN were systemically studied. The co-assembly of **L/D-PF1**/OFN and **L/D-PF2**/OFN displayed different chiroptical properties such as CD and CPL signals. Chirality transfer from the chirality center of **L/D-PF1** and **L/D-PF2** to the achiral OFN and chiral amplification were successfully achieved. Notably, a reversal phenomenon could be observed in **L/D-PF2**/OFN when the molar ratio changed from 1:1 to 1:2 while not found in **L/D-PF1**/OFN, indicating that minor structural changes of molecules could cause large changes in assembly. Besides, no significant CPL signal was observed in the self-assembly of **L/D-PF1** or **L/D-PF2** while co-assembly with OFN exhibited obvious CPL amplification induced by AP interaction. In particular, a reversal CPL signal was observed in **L/D-PF2/**OFN when the molar ratio changed from 1:1 to 1:2, which was consistent with Cotton effects. The dissymmetry factor g_{lum} could reach 5.5×10^{-3} (**L/D-PF1/**OFN = 1/2) and 6.3×10^{-3} (**L/D-PF2/**OFN = 1/1), which might be useful for the preparation of chiral matter. In addition, computational calculations such as MD simulation, NCI calculations, ESP and DFT calculations were conducted to verify the AP interaction between **L-PF1**/**L-PF2** and OFN. This work demonstrated that arene-perfluoroarene interaction could drive chiral transfer, chiral amplification and chiral inversion and provided a new method for the preparation of chiroptical materials.

Declaration of competing interest

The authors declare that they have no known competing financial interests or personal relationships that could have appeared to influence the work reported in this paper.

CRediT authorship contribution statement

Bo Luo: Writing – review & editing, Writing – original draft, Methodology, Investigation. **Mingfang Ma:** Resources, Methodology, Investigation, Formal analysis. **Aiyou Hao:** Visualization, Validation, Supervision, Resources. **Pengyao Xing:** Validation, Resources, Methodology, Funding acquisition, Conceptualization.

Acknowledgments

This work is financially supported by the National Natural Science Foundation of China (Nos. 22171165 and 22371170), Natural Science Foundation of Shandong Province (No. ZR2022MB080) and Scientific and Technological Frontiers in Project of Henan Province (No. 242102110192).

Supplementary materials

Supplementary material associated with this article can be found, in the online version, at doi:10.1016/j.cclet.2025.111736.

References

[1] G. Albano, G. Pescitelli, L. Di Bari, Chem. Rev. 120 (2020) 10145–10243.
[2] J. Kwon, K. Park, W. Choi, et al., Acc. Chem. Res. 56 (2023) 1359–1372.
[3] X. Niu, R. Zhao, S. Yan, et al., Small 19 (2023) 202303059.
[4] S. Jia, T. Tao, Y. Xie, et al., Small 20 (2023) 202307874.
[5] Y. Xia, A. Hao, P. Xing, Chin. Chem. Lett. 34 (2023) 107955.
[6] S. Huang, H. Yu, Q. Li, Adv. Sci. 8 (2021) 202002132.
[7] S. He, Z. Jiang, X. Dou, et al., ChemPlusChem 88 (2023) e202300226.
[8] C. Gao, Z. Zhu, S. Li, et al., Chin. Chem. Lett. 36 (2025) 109968.
[9] Y. Sun, Y. Jiang, J. Jiang, et al., Chin. Chem. Lett. 34 (2023) 108409.
[10] J. Li, P. Li, M. Fan, et al., Angew. Chem. Int. Ed. 61 (2022) e202202532.
[11] Q. Cheng, A. Hao, P. Xing, ACS Nano 18 (2024) 5766–5777.
[12] X. Wu, M. Liu, C. Zheng, et al., Chin. Chem. Lett. 34 (2023) 107590.
[13] C. Hao, G. Wang, C. Chen, et al., Nano-Micro Lett. 15 (2023) 39.
[14] S. Jiang, S. Zhou, Y. Chen, et al., Chin. Chem. Lett. 33 (2022) 2442–2446.
[15] S. Du, Y. Wang, F. Wang, et al., Chin. Chem. Lett. 35 (2024) 109256.
[16] Y. Liu, P. Xing, Adv. Mater. 35 (2023) 202300968.
[17] Z. Wang, A. Hao, P. Xing, Angew. Chem. Int. Ed. 62 (2022) e202214504.
[18] Z. Shen, Y. Sang, T. Wang, et al., Nat. Commun. 10 (2019) 3976.
[19] L. Zhang, H. Wang, S. Li, et al., Chem. Soc. Rev. 49 (2020) 9095–9120.
[20] D. Sahoo, R. Benny, N. Ks, et al., ChemPlusChem 87 (2021) e202100322.
[21] M. Hu, F. Ye, C. Du, et al., Angew. Chem. Int. Ed. 61 (2021) e202115216.
[22] Z. Wang, A. Hao, P. Xing, Chem. Mater. 35 (2023) 10178–10187.
[23] M. Hu, Y.X. Yuan, W. Wang, et al., Nat. Commun. 11 (2020) 161.
[24] W. Chen, L. Fu, Z. Zhu, et al., Chin. Chem. Lett. 34 (2023) 107713.
[25] G. Zhang, X. Cheng, Y. Wang, et al., Aggregate 4 (2022) e262.
[26] S. Penty, M. Zwijnenburg, G. Orton, et al., J. Am. Chem. Soc. 144 (2022) 12290–12298.
[27] Y. Zhang, X. Qin, X. Zhu, et al., Nat. Commun. 13 (2022) 7737.
[28] H. Jiang, L. Zhang, J. Chen, et al., ACS Nano 11 (2017) 12453–12460.
[29] Z. Geng, Y. Zhang, Y. Zhang, et al., Angew. Chem. Int. Ed. 61 (2022) e202202718.
[30] Y. Zhang, D. Li, Q. Li, et al., Adv. Funct. Mater. 33 (2023) 2309133.
[31] Y. Xia, A. Hao, P. Xing, Chin. Chem. Lett. 33 (2022) 4918–4923.
[32] L. Hu, K. Li, W. Shang, et al., Angew. Chem. Int. Ed. 59 (2020) 4953–4958.
[33] H. Zhang, J. Han, X. Jin, et al., Angew. Chem. Int. Ed. 60 (2021) 4575–4580.
[34] T. Kim, J. Hong, J. Kim, et al., J. Am. Chem. Soc. 145 (2023) 1793–1802.
[35] Y. Sun, Y. Lei, L. Liao, et al., Angew. Chem. Int. Ed. 56 (2017) 10352–10356.
[36] G. Lee, E. Hu, A. Rheingold, et al., J. Org. Chem. 86 (2021) 8425–8436.
[37] L. Wang, J. Deng, M. Jiang, et al., J. Mater. Chem. A 11 (2023) 11235–11244.
[38] X. Xia, Q. Lv, Y. Yu, et al., Sci. China Mater. 67 (2024) 946–953.
[39] Z. Feng, T. Hai, Y. Liang, et al., Angew. Chem. Int. Ed. 60 (2021) 27046–27052.
[40] A. Friedrich, I.E. Collings, K.F. Dziubek, et al., J. Am. Chem. Soc. 142 (2020) 18907–18923.
[41] S. An, M. Qiao, X. Jin, et al., Sci. China Chem. 67 (2023) 512–516.
[42] Z. Gu, W. Ma, J. Feng, et al., J. Phys. Chem. Lett. 14 (2023) 6437–6443.
[43] Y. Huang, Q. Gong, J. Ge, et al., ACS Nano 14 (2020) 15962–15972.
[44] Y. Huang, J. Xing, Q. Gong, et al., Nat. Commun. 10 (2019) 169.
[45] J. Liang, H. Zhang, A. Hao, et al., ACS Appl. Mater. Interfaces 13 (2021) 29170–29178.
[46] J. Zhao, B. Wang, A. Hao, et al., Nanoscale 14 (2022) 1779–1786.
[47] B. Liu, J. Gao, A. Hao, et al., Angew. Chem. Int. Ed. 62 (2023) e202305135.
[48] Q. Cheng, A. Hao, P. Xing, Chem. Sci. 15 (2024) 618–628.